Received: 14 March 2024 | Revised: 22 August 2024 | Accepted: 26 August 2024

DOI: 10.1002/hbm.70021

RESEARCH ARTICLE

WILEY

Language networks of normal-hearing infants exhibit topological differences between resting and steady states: An fNIRS functional connectivity study

Ishara Paranawithana[1,2] | Darren Mao[2,3] | Colette M. McKay[2,3] | Yan T. Wong[1,4]

[1]Department of Electrical and Computer Systems Engineering, Monash University, Clayton, Victoria, Australia

[2]Bionics Institute, East Melbourne, Victoria, Australia

[3]Department of Medical Bionics, The University of Melbourne, Parkville, Victoria, Australia

[4]Department of Physiology and the Monash Biomedicine Discovery Institute, Monash University, Clayton, Victoria, Australia

Correspondence
Yan T. Wong, Department of Physiology and the Monash Biomedicine Discovery Institute, Monash University, Clayton, Victoria 3800, Australia.
Email: yan.wong@monash.edu

Funding information
Medical Research Future Fund (BioMedTech Horizons Program); Victorian Medical Research Acceleration Fund; National Health and Medical Research Council, Grant/Award Number: GNT1154233

Abstract

Task-related studies have consistently reported that listening to speech sounds activate the temporal and prefrontal regions of the brain. However, it is not well understood how functional organization of auditory and language networks differ when processing speech sounds from its resting state form. The knowledge of language network organization in typically developing infants could serve as an important biomarker to understand network-level disruptions expected in infants with hearing impairment. We hypothesized that topological differences of language networks can be characterized using functional connectivity measures in two experimental conditions (1) complete silence (resting) and (2) in response to repetitive continuous speech sounds (steady). Thirty normal-hearing infants (14 males and 16 females, age: 7.8 ± 4.8 months) were recruited in this study. Brain activity was recorded from bilateral temporal and prefrontal regions associated with speech and language processing for two experimental conditions: resting and steady states. Topological differences of functional language networks were characterized using graph theoretical analysis. The normalized global efficiency and clustering coefficient were used as measures of functional integration and segregation, respectively. We found that overall, language networks of infants demonstrate the economic small-world organization in both resting and steady states. Moreover, language networks exhibited significantly higher functional integration and significantly lower functional segregation in resting state compared to steady state. A secondary analysis that investigated developmental effects of infants aged 6-months or below and above 6-months revealed that such topological differences in functional integration and segregation across resting and steady states can be reliably detected after the first 6-months of life. The higher functional integration observed in resting state suggests that language networks of infants facilitate more efficient parallel information processing across distributed language

regions in the absence of speech stimuli. Moreover, higher functional segregation in steady state indicates that the speech information processing occurs within densely interconnected specialized regions in the language network.

KEYWORDS
functional connectivity, functional near-infrared spectroscopy, graph network measures, language networks, resting state, small-world topology, steady state

1 | INTRODUCTION

The auditory and language brain regions perform sensory processing and perception tasks using a complex network of structurally and functionally interconnected cortico-cortical neuronal connections (Friederici, 2012; Hickok & Poeppel, 2007; Weiss-Croft & Baldeweg, 2015). There is evidence in support of the premise that those connections in language networks could be severely disrupted due to complete absence or weakened auditory input in children born with hearing impairment (Jung et al., 2017; Sharma & Cardon, 2014; Shi et al., 2016; Wang et al., 2019). Therefore, delayed medical intervention for hearing loss can have a profound effect on how children develop speech and language. Moreover, previous studies have shown that language networks of normal-hearing individuals also undergo a range of spatiotemporal changes with development during early childhood (Aslin, 1980; Emerson et al., 2016; Gao et al., 2011; Gao et al., 2015; Polka & Werker, 1994; Saffran et al., 1996; Werker & Tees, 1984). Therefore, understanding the underlying principles of functional organization of language networks is fundamental to determining the effects of hearing impairment on speech and language development.

The field of functional connectivity has gained much attention in the recent past due to its promise in characterizing the functional organization of the brain using non-invasive brain imaging techniques (Bullmore & Sporns, 2009; Fox & Greicius, 2010). To this end, functional near-infrared spectroscopy (fNIRS) has been an attractive and widely used optical functional neuroimaging technique (Ayaz et al., 2022; Lu et al., 2010). fNIRS infers brain activity indirectly by measuring hemodynamic responses due to neurovascular coupling in terms of oxy-hemoglobin (HbO) and deoxy-hemoglobin (HbR) concentration changes (Ferrari & Quaresima, 2012; Scholkmann et al., 2014). fNIRS also offers several advantages over fMRI as it is less expensive, portable, child-friendly, and less sensitive to motion artifacts (Pinti et al., 2020). Compared to fMRI, having higher temporal resolution and being a silent neuroimaging technique, fNIRS is a preferred alternative for studies investigating neural mechanisms of auditory and language processing using resting state data. Moreover, resting state fNIRS has been extensively used with infants and young children who often have difficulty in performing task-related activities (Blanco et al., 2021; Bulgarelli et al., 2020; Hu et al., 2020; Paranawithana et al., 2023a).

Previous fNIRS functional connectivity studies have largely used either the approach of seed-based correlation or independent component analysis (Zhang, Lu, et al., 2010; Zhang, Zhang, et al., 2010). Using such techniques, several studies have demonstrated connectivity patterns consistent with fMRI findings in visual, auditory, sensorimotor systems in many subject populations including infants (Bulgarelli et al., 2018) and adults (Duan et al., 2012; Paranawithana et al., 2022; White et al., 2009). More recently, a graph theoretical approach has been adopted in structural and functional neuroimaging studies (Bullmore & Bassett, 2011; Bullmore & Sporns, 2009) to quantify and characterize topological properties of brain networks. The application of graph network measures has revealed that brain networks possess many interesting underlying topological principles such as small-worldness, modularity and hubness (Achard & Bullmore, 2007; Bassett & Bullmore, 2006; Bullmore & Sporns, 2012; Niu et al., 2012; Niu et al., 2013). More importantly, graph network analysis has proven to be useful in tracking connectivity changes due to typical development in childhood (Cai et al., 2018; Liu et al., 2022) and aging (Dennis & Thompson, 2014) and detecting alterations of connectivity patterns in neuropathological conditions (Bassett & Bullmore, 2009; Zhang et al., 2018; Zhang et al., 2022).

Task-related studies have consistently reported significant activations in response to speech sounds (Dehaene-Lambertz et al., 2006; Mao et al., 2021; Shader et al., 2021) in regions associated with language processing such as primary auditory cortex in the temporal lobe and inferior frontal gyrus (IFG) in the frontal lobe. Previous functional connectivity studies have reported the presence of small-world topology in primary and higher order brain networks of adults, young children, and infants (Cai et al., 2018; Liu et al., 2022; Niu et al., 2012; Oldham & Fornito, 2019). However, these studies mainly focused on investigating large-scale resting state networks and have not considered or compared against networks derived from task-evoked activity. Therefore, topological differences of language networks when processing speech sounds compared to resting state largely remain unclear. Moreover, topological changes with development in the early critical period for language development of the first 2 years of life are not well understood (Weiss-Croft & Baldeweg, 2015; Zhang et al., 2019).

In this study, we hypothesized that topological differences of language networks in different conditions can be characterized using graph network measures derived from fNIRS-based functional connectivity. To test the hypothesis, we conducted an experiment with two experimental conditions namely resting and steady states on children under 2 years of age with normal-hearing. While the resting state was the standard silent paradigm in the absence of an overt task/

stimulus, a repetitive speech sound was presented in a continuous manner in steady state. fNIRS data were recorded from bilateral temporal and prefrontal regions and graph network measures of global efficiency, local efficiency, characteristic path length and clustering coefficient were used to characterize small-world properties in resting and steady states at group-level. Further, the normalized global efficiency and clustering coefficient were used as measures of functional integration and segregation, respectively to assess topological differences of two conditions at individual subject-level. The participants were divided into two groups as (1) 6-months or below and (2) above 6-months to further investigate potential developmental effects of functional organization during early childhood. The knowledge of typical functional mechanisms of language networks in normal-hearing infants could serve as a potential biomarker to better understand network-level dysfunction expected in infants with hearing impairment.

2 | METHODS

2.1 | Participants

Thirty babies with normal-hearing (14 males and 16 females, mean and standard deviation of age: 7.8 ± 4.8 months, age range: 2–21 months) participated in this study. Three babies were born prematurely (gestational age <38 weeks). None of the participants had major complications during pregnancy or known cognitive and/or developmental disorder at the time of testing. All participants were included in the analysis considering the chronological or corrected gestational age for full-term and pre-term babies, respectively (Table S1). All infants had passed either a newborn hearing screening test or follow-up diagnostic audiology assessments. Tympanometry was performed on the day of testing with probe tone 226 Hz for babies above 6-months and 1000 Hz for infants under 6-months to ensure that participants did not have temporary conductive hearing loss. The study was approved by the human research ethics committee of the Royal Children's Hospital (71941) in Melbourne. Written informed consent was obtained from the parents before the start of the experiment.

2.2 | Experimental procedure and protocol

The experiments were conducted in a dimly lit sound attenuated room. The parent was seated in a comfortable armchair cradling the baby during the testing. They were given time to feed and settle the baby and the data collection started after confirming that the infant was in sound sleep and approximately at the same time of the sleep cycle for all participants. The parents were instructed to limit their body movements as much as possible to make sure infants remained asleep throughout the experiment. The experimental protocol was designed with two recording phases, (1) without and (2) with speech sound presentation. The protocol started with a standard "resting state" recording conducted in complete silence. In contrast to the resting state, a standard speech sound ("*Baa*" sound) was presented repetitively to habituate responses to a non-silence baseline in the second phase of the protocol. This experimental condition with repeated "*Baa*" sound is referred to as "steady state" in this study.

The two experimental conditions used in this study which had either continuous silence or continuous presentation of speech sounds are illustrated in Figure 1c. Five minutes of data were recorded for each condition during the same experiment session for each participant with a time gap between the two conditions. A consonant-vowel syllable of "*Baa*" sound was specifically selected as the speech stimulus in the steady state as it is a common speech sound used in speech discrimination studies (de la Cruz-Pavía & Gervain, 2023; Nakano et al., 2009). For more details about the rationale and development of the experimental protocol, interested readers may refer to our previous study (Mao et al., 2021; McKay et al., 2023). The speech stimulus was generated by a female native Australian English speaker. The stimulus was 500 milliseconds in duration, recorded at a sampling rate of 44.1 kHz, equalized in root- mean-square amplitude. By concatenating 600 identical speech sounds, a continuous stimulus of 5 min was presented to the participants using ER3 insert-phones (Etymotic Research, Inc., USA) at 65 dB SPL.

2.3 | Data acquisition

The optode montage was designed in NIRSite software (NIRx Medical Technologies, LLC, USA) using a 2–5 months-old infant brain atlas. To ensure that optode montage coverage is within auditory and language regions, channel coordinates were registered on a 0–2-year-old AAL atlas using devfOLD toolbox (Fu & Richards, 2021). The source and detector locations based on the modified combinatorial nomenclature, MNI coordinates of channels, anatomical label of the contributing brain region and the specificity of each channel are presented in Table 1. Before the start of the experiment, each participant was fitted with an appropriately sized flexible headcap (EasyCap, Brain Products GmbH, Germany) after measuring the head circumference. The headcap and optode positions were checked with respect to known anatomical landmarks of the modified combinatorial nomenclature. Flat tip optodes were used to reduce scalp irritation and provide enhanced safety and comfort for infants. The source-detector pairs were placed 2–3 cm apart (mean and standard deviation of source-detector separation: 2.3 ± 0.2 cm).

A multi-channel continuous wave fNIRS system (NIRScout, NIRx Medical Technologies, LLC, USA) was used to record brain activity. This laboratory-grade fNIRS system uses light emitting diodes (LEDs), operating at two near-infrared wavelengths (760 and 850 nm) as sources and high sensitivity avalanche photodiodes (APDs) as detectors. Eight sources and eight detectors were placed over bilateral temporal and prefrontal regions covering brain regions associated with speech and language processing as shown in Figure 1a. These two regions of interest largely covered brain areas which are known to be associated with speech and language processing including Wernicke's (Brodmann's area, BA 22 and 40) and Broca's area (BA 44 and 45).

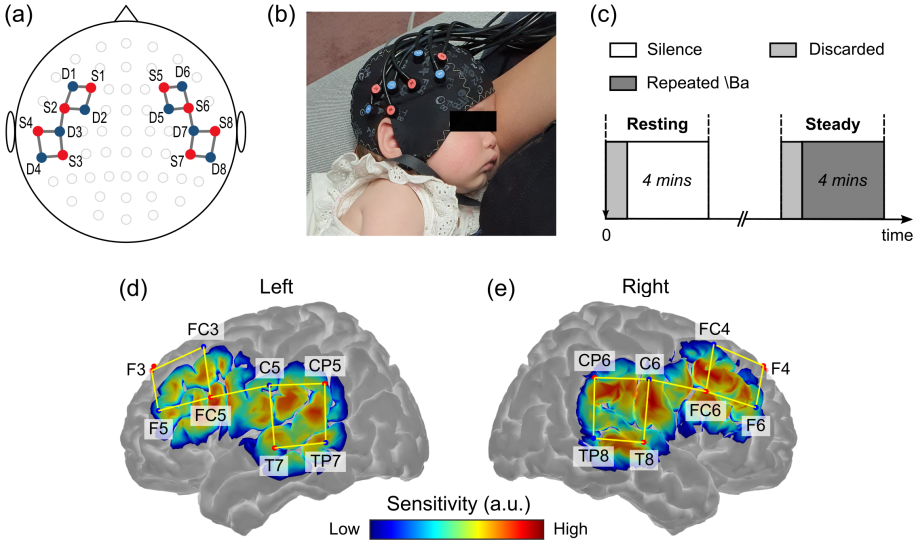

FIGURE 1 (a) The 2D view of the optode montage. The optodes are placed on bilateral prefrontal and temporal areas forming 18 fNIRS channels (indicated by grey straight lines). Sources (S) and detectors (D) are marked in red and blue filled circles, respectively. (b) An image of an infant taken during the experiment showing optode positions on the headcap. (c) Illustration of the experimental protocol used in the study. Each experimental condition (resting and steady) had 5 min of continuous recording and the first minute of data were discarded in both states. The sensitivity profile of fNIRS probes in (d) left and (e) right hemispheres with warmer and cooler colours indicating high and low sensitivity, respectively.

TABLE 1 fNIRS channel coordinates and contributing brain regions based on the channel registration on a 0–2-year-old AAL atlas.

ROI	Ch #	Source-detector	MNI channel coordinates	Anatomical label	Specificity (%)
Left frontal	1	F3-FC3	−50, 21, 44	Frontal_Mid_2_L	78.04
	2	F3-F5	−51, 34, 31	Frontal_Mid_2_L	65.62
	3	FC5-FC3	−60, 9, 35	Precentral_L	42.62
	4	FC5-F5	−60, 21, 21	Frontal_Inf_Tri_L	64.31
	5	FC5-C5	−69, −6, 20	Postcentral_L	36.02
Left temporal	6	CP5-C5	−71, −33, 21	Temporal_Sup_L	58.81
	7	CP5-TP7	−69, −44, 6	Temporal_Mid_L	62.22
	8	T7-C5	−72, −18, 3	Temporal_Sup_L	51.31
	9	T7-TP7	−70, −30, −12	Temporal_Mid_L	57.89
Right frontal	10	F4-FC4	47, 21, 45	Frontal_Mid_2_R	81.30
	11	F4-F6	48, 35, 32	Frontal_Mid_2_R	65.67
	12	FC6-FC4	58, 8, 36	Frontal_Inf_Oper_R	30.38
	13	FC6-F6	58, 20, 22	Frontal_Inf_Tri_R	74.80
	14	FC6-C6	66, −7, 20	Postcentral_R	41.59
Right temporal	15	CP6-C6	68, −34, 21	Temporal_Sup_R	31.04
	16	CP6-TP8	66, −45, 7	Temporal_Mid_R	79.31
	17	T8-C6	69, −19, 3	Temporal_Mid_R	68.28
	18	T8-TP8	68, −32, −12	Temporal_Mid_R	58.77

Note: The specificity cutoff was set to 15% and the anatomical label with the highest specificity value is reported for each channel.
Abbreviations: Ch #, channel number; ROI, region of interest.

The optode montage had a total of 18 fNIRS channels and each channel recorded data at a sampling rate of 15.625 Hz. The mirrored sources on left and right hemispheres were switched on at the same time using a bilateral illumination sequence.

2.4 | Data pre-processing

Data pre-processing and statistical analysis were conducted in Matlab R2022b (Mathworks Inc., USA). A combination of in-built functions

and customized scripts were used in the data pre-processing stage. In-built functions from Matlab-based open-source toolbox (NIRS Brain AnalyzIR toolbox (Santosa et al., 2018) also known as nirs-toolbox, version 837) were primarily used for fNIRS-specific signal conditioning and pre-processing. fNIRS signals were recorded in raw format as light intensity data and all the pre-processing was carried out entirely off-line. The first step of the pre-processing pipeline was to insert dummy event triggers at 20 second intervals. This was done to automate the data extraction process by discarding irrelevant event tokens systematically and maintain a consistent workflow for all participants. Having dummy triggers facilitated in creating data epochs and performing signal quality assessment for smaller time windows instead of considering the entire timeseries signal at once. Four-minutes of data were considered in the analysis for each state and each participant after discarding the data of first minute, consistent with previous fMRI/fNIRS studies (Aarabi & Huppert, 2019; Bulgarelli et al., 2020; Homae et al., 2010; Paranawithana et al., 2023b). The aim of discarding data was to allow enough time for responses to return to baseline levels and minimize transitioning effects due to the changeover in experimental conditions.

fNIRS channels with poor signal quality were identified using the following quality assessment criteria and labelled to be excluded from further analysis. First, a quality metric was applied during the calibration stage prior to recording data to ensure the amount of light received by the detectors is within an acceptable range. Any channel with a gain factor of 0 or 8, intensity level of 0.01–0.03 or >2.5 V and noise >7.5% was marked as "critical" by the signal acquisition software (NIRStar, NIRx Medical Technologies, USA). The scalp coupling index (SCI) was used as the second quality metric in the data pre-processing stage. This metric considers the presence of cardiac signal in fNIRS data (or lack thereof) as an indicator to measure the quality of contact between the scalp and optodes. The timeseries signals were bandpass filtered in the frequency band of 1.5–3 Hz to isolate cardiac content (zero-phase IIR Butterworth filter with a filter order of 8). The SCI was defined as the correlation between signals of two optical wavelengths in the cardiac frequency band. The quality metric was calculated for each epoch and each channel and channels with an epoch-averaged SCI value below 0.8 were rejected as shown in Figure S1. Setting this threshold ensured the number of channels that were not attributed to activity from a physiological origin remained low (mean and standard error of the percentage of rejected channels across participants: 4.5 ± 1.4% and 6.7 ± 1.8% for resting and steady state, respectively).

The following pre-processing steps were applied to convert raw data into hemodynamic responses. First, raw light intensity data were transformed to optical densities attributed to two distinct wavelengths. Then, motion artifact correction was performed by using two standard techniques commonly used in fNIRS data pre-processing. To correct for sudden shifts in signal amplitude possibly due to the displacement of optodes, the temporal derivative distribution repair (TDDR) algorithm (Fishburn et al., 2019) was applied. The algorithm processed positive and negative derivatives separately to downweigh outliers. A wavelet filter was then employed to correct spike-like artifacts which could be directly related to sudden movements of the head or residual spikes after applying the TDDR algorithm. The wavelet filter was designed using 'Sym8' wavelet basis function and the outliers were defined as coefficients outside four standard deviations from the mean. Motion artifact corrected optical densities were then converted to HbO and HbR concentration changes using the modified Beer–Lambert law (Delpy et al., 1988). To reduce the effect of high-frequency systemic physiological noise such as respiration and heartbeat and artifacts related to the very low frequency drift, we bandpass filtered signals in 0.01–0.1 Hz frequency band. Due to the slow nature of hemodynamic responses, we isolated low frequency oscillations below 0.1 Hz consistent with previous fNIRS studies (Biswal et al., 1995; Fox & Raichle, 2007; Lu et al., 2010). A representative example of filtered time series signals for left temporal and right temporal regions of interest are shown in Figure 2b.

2.5 | Construction of networks and graph theoretical analysis

Many studies have used graph theory as a promising model-free approach to characterize the topological organization of functional networks of the human brain (Cai et al., 2018; Zhang et al., 2018; Zhang et al., 2022). In this study, we adopted graph theoretical measures to quantify network-level topological differences between resting and steady states. The nodes of the graph were defined as fNIRS measurement channels, and the edges were the binarized functional connectivity indicating the presence or absence of connections between each pair of nodes. The graph construction and network analysis were performed in FC-NIRS, a Matlab-based functional connectivity toolbox (NeuroImaging Tools and Resources Collaboratory, 2023; Xu et al., 2015).

We used Pearson's correlation coefficient as the measure of functional connectivity strength. First, pairwise correlations were calculated between filtered HbO timeseries signals of all possible channel pairs, resulting in a 18 × 18 correlation matrix for each condition and each participant. Next, binary graphs (i.e., adjacency matrices) were constructed for each condition and each participant after thresholding correlation matrices over the full range of positive correlations. The channels with poor signal quality identified in the data pre-processing stage were removed from connected graphs by replacing them with zeros. The network analysis was restricted to only positive correlations due to the ambiguity on physiological interpretation of negative correlations (Fox et al., 2009; Weissenbacher et al., 2009). However, the proportion of negative correlations excluded from the network analysis was relatively low (5.6% and 7.2% of all pairwise correlations for resting and steady state, respectively). Setting a predefined single threshold is challenging due to the limited knowledge about the topology of language networks, particularly true for infants and young children. Therefore, thresholding was performed over the full correlation range (0.01–0.99) at increments of 0.01 as suggested by previous studies (Bullmore & Bassett, 2011; Bullmore & Sporns, 2009). Following this standard approach minimizes spurious effects in network topology due to the ambiguity of choosing a single threshold.

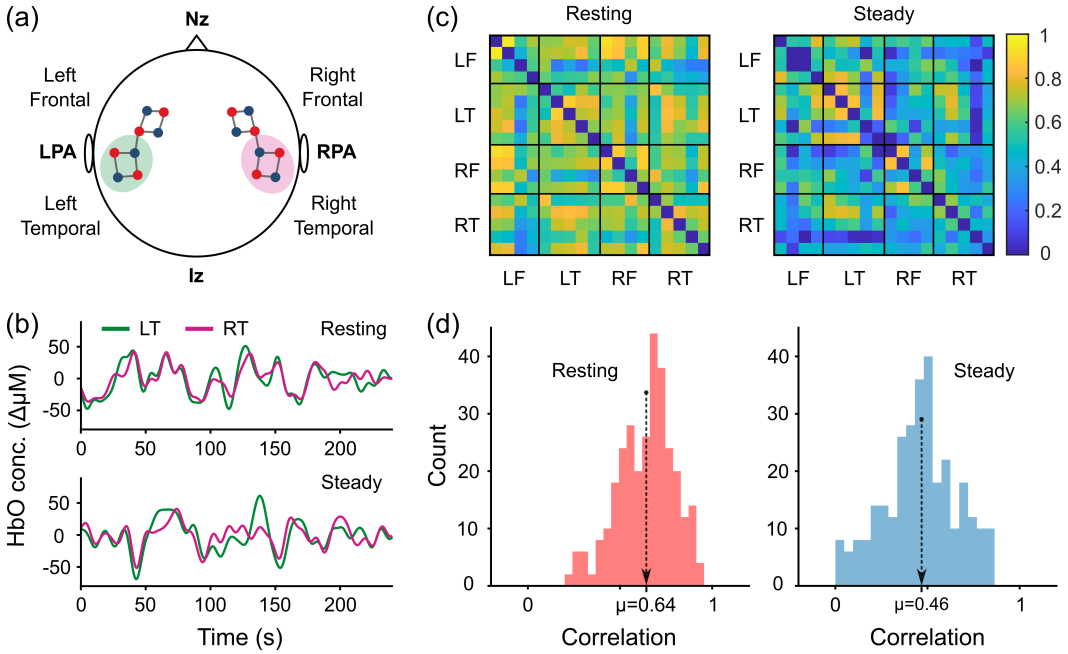

FIGURE 2 (a) The optode montage with four distinct regions of interest namely, left frontal (LF), left temporal (LT), right frontal (RF), right temporal (RT) and anatomical landmarks; left pre-auricular point (LPA) and right pre-auricular point (RPA). The left and right temporal regions of interest associated with auditory and language processing are highlighted green and pink circles, respectively. (b) Group-level representative examples of HbO timeseries signals averaged across channels in each region of interest (color-coded) for resting and steady states. (c) Group-level association matrices (correlation maps) of resting and steady states after excluding a smaller proportion of negative correlations. (d) Correlation distributions of two experimental conditions demonstrating higher overall connectivity strength in resting state compared to steady state.

Graph network measures can be greatly influenced by topological factors such as the number of nodes, edges, and the degree distribution of the network (Rubinov & Sporns, 2010; Zalesky, Fornito, & Bullmore, 2010). To compare network characteristics and establish statistical significance of real brain networks (Bullmore & Sporns, 2009; Rubinov & Sporns, 2010), we used networks with a random topology as null-hypothesis models. Real brain networks were compared against 1000 matched random null networks maintaining the same number of nodes, edges, and degree distribution as the real network. Four graph network measures were used to characterize the topological organization and differences in functional properties between resting and steady states of language networks. Those are characteristic path length (L_p), global efficiency (E_g), clustering coefficient (C_p), and local efficiency (E_{loc}) of the network. Characteristic path length and global efficiency were used as measures of functional integration while functional segregation was measured using clustering coefficient and local efficiency (Bullmore & Sporns, 2012; Rubinov & Sporns, 2010). The characteristic path length is defined as the average shortest path length of a network. It can be computed as:

$$L_p = \frac{1}{N(N-1)} \sum_{i \neq j \in G} d_{ij} \tag{1}$$

where d_{ij} is the shortest path length between node i and node j, N is the number of nodes of a network represented by graph G. The clustering coefficient reflects the ability of the network to cluster together in subgraphs with higher clustering implying greater segregation. The clustering coefficient can be expressed as:

$$C_p = \frac{1}{N} \sum_{i \in G} \frac{G_i}{k_i(k_i-1)/2} \tag{2}$$

where G_i is the subgraph of neighbors of node i and k_i denotes the number of neighbors of node i. To evaluate the information exchange capacity across nodes of the network, network efficiency can be computed at global and local levels. The global efficiency is defined as the average inverse shortest path length and the local efficiency of a network can be represented as the global efficiency of the subgraph composed of the nearest neighbours to node i. These measures can be calculated as:

$$E_g = \frac{1}{N(N-1)} \sum_{i \neq j \in G} (d_{ij})^{-1}. \tag{3}$$

$$E_{loc} = \frac{1}{N} \sum_{i \in G} E_g(i) \tag{4}$$

where $E_g(i)$ refers to the global efficiency of G_i.

To further explore small-world properties of the networks, normalized network measures were calculated by considering the ratios between real and random networks for each condition. A small-world network is characterized as a network having much greater clustering coefficient and similar average shortest path length compared to a

random network. This can be mathematically represented as $\gamma \gg 1$ and $\lambda \approx 1$, where $\gamma = C_p^{real}/C_p^{rand}$ and $\lambda = L_p^{real}/L_p^{rand}$. Similarly, normalized metrics for efficiencies were computed as $\gamma_E = E_{loc}^{real}/E_{loc}^{rand}$ and $\lambda_E = E_g^{real}/E_g^{rand}$ where γ_E and λ_E are normalized local and global efficiency, respectively. All network measures considered were important in explaining the characteristics of small-world topology for the whole correlation range. However, due to the redundancy of information, we only considered the normalized global efficiency and clustering coefficient as representative measures of functional integration and segregation, respectively for further statistical analysis. The mean of each normalized network measure over the full range of correlations was used as a threshold-independent scalar for statistical comparisons of functional differences. The statistical analysis was conducted using one-sided paired Wilcoxon signed rank test to determine if there were significant differences in functional integration and segregation of language networks across two experimental conditions. For all statistical tests, we used the significance level of 0.05 for falsely rejecting the null hypothesis.

To identify which functional connections differ in connectivity strengths between two experimental conditions, we conducted both qualitative and quantitative analysis. First, a qualitative analysis was performed using BrainNet Viewer (Xia et al., 2013) by visualizing the weighted and undirected connectivity maps for resting and steady states separately. Group-level connectivity matrices were generated by averaging correlations over threshold bins (0.01–0.99) for each participant and then across participants. A correlation cutoff of 0.5 was used to retain the suprathreshold weights and exclude weak and/or spurious connections. The choice of threshold cutoff was based on the observations in Section 3.1 where expected features of small-world topology were more prominent after the correlation threshold of 0.5.

We used network-based statistics (NBS) toolbox (Zalesky, Fornito, Harding, et al., 2010) to quantitatively examine differences in functional connectivity strengths between resting and steady states. The NBS was designed to identify effects in the topological space by comparing connectivity strengths across conditions using a mass univariate testing model at the edge level. In our study, a paired t-test was used to determine pairwise differences of connectivity strengths between resting and steady states. The statistical significance was established by running 5000 permutations and setting the familywise error rate at 0.05. The randomization of connections in the permutation test was constrained to the repeated measures of the same subject. A test statistic threshold of 2.1 was used for each pairwise association to select a set of supra-threshold connections. The size of the connected graph component was measured using intensity (mass) similar to the supra-threshold voxel clustering explained in a previous study (Bullmore et al., 1999).

In a secondary analysis, the participants were separated into two groups based on age to investigate developmental effects in functional integration and segregation of language networks between resting and steady state conditions. Each group had fifteen participants with the following subject demographics: (1) 6-months or below (7 males and 8 females, mean and standard deviation of age: 4.1 ± 1.4 months) and (2) above 6-months (7 males and 8 females, mean and standard deviation of age: 11.6 ± 3.9 months). The grouping of participants was motivated by perceptual milestones of language development reported in previous studies (Aslin, 1980; Saffran et al., 1996; Werker, 2024; Werker & Tees, 1984). Those studies have shown that the reorganization from language-general to language-specific phonetic discrimination mostly occurs in the second half of the first year and infants begin to specialize in the sounds of their native language between 6 and 12 months of age (Polka & Werker, 1994). The same analytical framework described in the previous section was applied for the secondary analysis.

3 | RESULTS

3.1 | Functional language networks demonstrate economic small-world properties in both resting and steady states

Economic small-world property is an attractive feature for language networks because this topology enables networks to process information in a highly modularized and distributed manner simultaneously. We assumed that language networks of infants which are a subset of whole brain networks would show an economic small-world organization. To test the hypothesis that language networks of infants demonstrate economic small-world properties in both resting and steady states, we computed graph network measures as a function of correlation for two experimental conditions separately. The profiles of participant averaged small-world parameters (clustering coefficient and characteristic path length) and network efficiencies (local efficiency and global efficiency) as a function of correlations for resting and steady state conditions are shown in Figure 3a–d. As expected, the clustering coefficient monotonically decreased while characteristic path length monotonically increased with the correlation threshold for both real and random networks of resting and steady state conditions. It can be observed that networks have smaller clustering coefficients and longer path lengths at higher correlation thresholds due to the retention of supra-thresholded connections. As thresholds increase, networks become sparser and more heterogeneous, shifting towards a more complex architecture demonstrating small world properties.

The curves of clustering coefficients for random networks were consistently below those of the real networks whereas characteristic path lengths of real and random networks had similar trajectories in both resting and steady states. Both global and local efficiency measures of real networks and matched random networks decreased as the correlation threshold increased for resting state. A similar pattern was observed for steady state indicating higher network efficiency for lower cost. However, the local efficiency of real networks was higher than the matched random networks for the whole range of correlation thresholds. In contrast, we observed that the global efficiency of real networks was lower than the equivalent random networks for low to medium cost. Nevertheless, the global efficiency of real networks was numerically similar compared to that of random networks.

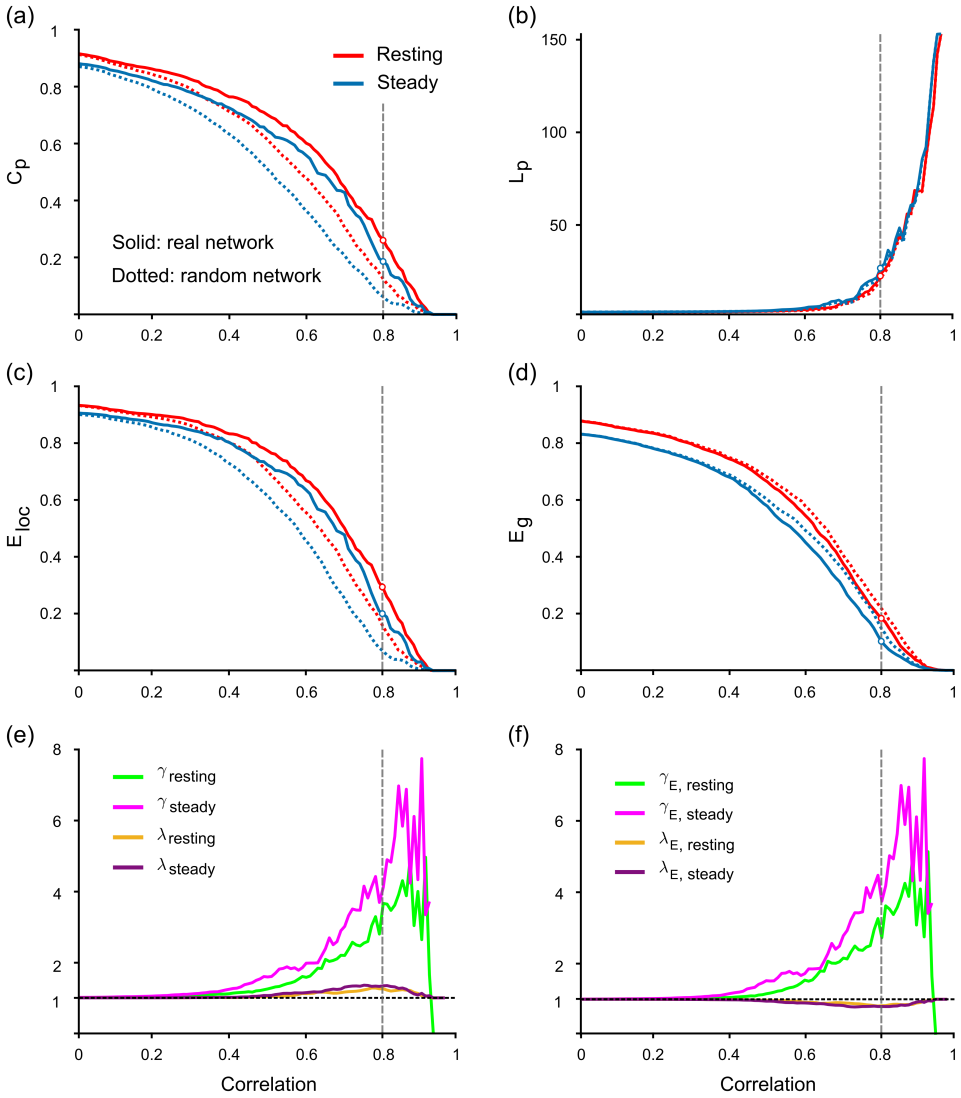

FIGURE 3 The small-world properties and efficiency characteristics for functional networks constructed from HbO signals of resting and steady states. Participant-averaged network measures of (a) clustering coefficient (C_p), (b) characteristic path length (L_p), (c) global efficiency (E_g) and (d) local efficiency (E_{loc}) are shown as a function of correlation thresholds for resting and steady states and real networks (solid lines) as well as 1000 matched random null networks (dotted lines). Normalized (e) small-world properties and (f) global and local efficiencies for both experimental conditions demonstrate typical features of small-world topology ($\gamma \gg 1$ and $\lambda \approx 1$). The dashed vertical line in each panel indicates a cross-sectional representative example of network metrics for a sparse and heterogenous network with a threshold of 0.8.

The normalized small-world properties and network efficiencies as a function of correlation are shown in Figure 3e and Figure 3f, respectively. For both resting and steady states, the normalized clustering coefficients ($\gamma_{resting}$ and γ_{steady}) were observed to be much greater than 1 while normalized characteristic path lengths ($\lambda_{resting}$ and λ_{steady}) were closer to 1, prominently for higher correlation thresholds, demonstrating the properties of small-world organization. The normalized local and global efficiency profiles of resting and steady states demonstrated similar patterns with local efficiency ($\gamma_{E,resting}$ and $\gamma_{E,steady}$) higher than 1 and global efficiency ($\lambda_{E,resting}$ and $\lambda_{E,steady}$) closer to 1.

A comparison of normalized metrics from a cross-sectional representative example of heterogenous network (thresholded at 0.8) is reported in Table 2. Based on this representative example, we can observe that the normalized clustering coefficient of steady state networks is higher than that of the resting state networks. However, the resting state networks exhibited a higher normalized global efficiency compared to steady state. Overall, the results demonstrated greater functional segregation and comparable functional integration in real networks with respect to a set of matched random networks exhibiting typical features of economic small-world topology. These observations at group-level suggested that language networks maintain distributed and localized information processing capabilities in both experimental conditions. These findings are consistent with previous fMRI resting state studies that showed the presence of small-world organization in brain networks in early childhood (Gao et al., 2011; Zhang et al., 2019).

TABLE 2 Normalized network measures of a representative example network thresholded at a higher correlation cutoff of 0.8, yielding a heterogenous complex network architecture.

Normalized metric	Resting	Steady
Clustering coefficient (γ)	3.66 ± 0.77	4.11 ± 0.58
Characteristic path length (λ)	1.26 ± 0.05	1.34 ± 0.07
Local efficiency (γ_E)	3.63 ± 0.79	4.19 ± 0.62
Global efficiency (λ_E)	0.82 ± 0.03	0.80 ± 0.04

Note: The results are represented as mean ± 1 SE of the mean of each metric for two experimental conditions.

3.2 | Language networks of infants exhibit differences in functional topology across resting and steady states

To further examine the differences in functional topology at the individual subject-level, we used normalized global efficiency and clustering coefficient which are measures of functional integration and segregation, respectively. Non-parametric one-sided paired-sample statistical tests were conducted for each metric separately to test paired differences across resting and steady states. We hypothesized that the language network would be more functionally integrated in resting state compared to steady state. This is due to the need for more distributed information processing in resting state in the absence of external speech stimuli as opposed to steady state. Contrarily, a higher functional segregation was expected in steady state compared to resting state based on the assumption that more functionally specialized clusters within the language network would be required to process repetitive speech sounds.

Two normalized graph network measures (global efficiency and clustering coefficient) averaged over the entire correlation sequence were used as representative metrics of functional organization as shown in Figure 4. Using the mean of normalized parameters for each participant, we aimed to characterize functional differences of real brain networks relative to a group of matched random graphs at the individual subject-level. While the normalized global efficiency of both conditions was close to 1 (resting mean: 0.95; steady mean: 0.93), we can observe that both mean and median across participants were higher in resting compared to steady state. A paired Wilcoxon signed-rank test confirmed that global efficiency is significantly higher in resting state compared to steady state ($Z = 1.83$, $p = 0.03$). This result indicates that greater functional integration is present in resting state than steady state, possibly to facilitate distributed information processing.

The normalized clustering coefficient of resting and steady state conditions demonstrated an inverse pattern. As expected, the normalized clustering coefficient was >1 on average for both conditions (mean resting: 1.57; mean steady: 1.89). The statistical test revealed that the normalized clustering coefficient of resting state is significantly lower than that of steady state ($Z = -1.87$, $p = 0.03$). Since a higher clustering coefficient implies greater functional segregation, the results suggested that language networks of infants are more functionally localized when processing speech sounds in steady state compared to resting state. Taken together, the findings highlight the important fact that language networks exhibit differences in functional organization in response to silence versus continuous auditory stimuli presented as repetitive speech sounds.

3.3 | Inter-hemispheric and left intra-hemispheric long-distance connections are stronger in resting state than steady state

From group-level correlation distributions, we observed that the connection strength is generally higher in resting state compared to steady state. The qualitative results from BrainNet Viewer suggested that the resting state connections are stronger, and the network is denser compared to steady state as shown in Figure 5a-b. This was a prominent observation for both long-range inter-hemispheric and long-range intra-hemispheric connections of the language network. The inter-hemispheric connections in resting state were more evenly distributed for both frontal and temporal homologous regions. However, relatively fewer inter-hemispheric homologous connections between temporal regions were observed in steady state. Interestingly, while intra-hemispheric long-distance connections in the right hemisphere were similar in two conditions, we observed an increase in the number of connections between left frontal and left temporal regions in resting state than steady state. These qualitative results are consistent with the results obtained from graph network analysis, indicating efficient information processing across distributed language regions with greater functional integration in resting state compared to steady state.

In the quantitative analysis conducted using NBS toolbox, we hypothesized that the connectivity strengths of resting state connections are higher compared to those of steady state. The subnetwork shown in Figure 5c represents links which are significantly stronger in resting state than steady state based on NBS results. Consistent with

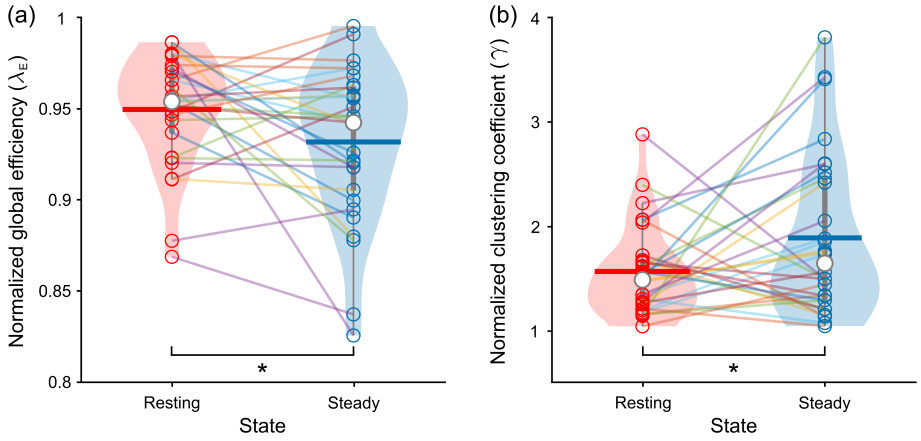

FIGURE 4 Violin plots of (a) normalized global efficiency and (b) clustering coefficient averaged over the entire correlation sequence as threshold-independent measures of functional integration and segregation, respectively. Each circle represents an individual participant of resting state in red and steady state in blue. Horizontal bold lines indicate group mean and white filled circles denote median of each network metric. Non-parametric statistical tests were conducted using one-sided paired Wilcoxon signed-rank test and the notation * indicates $p < 0.05$.

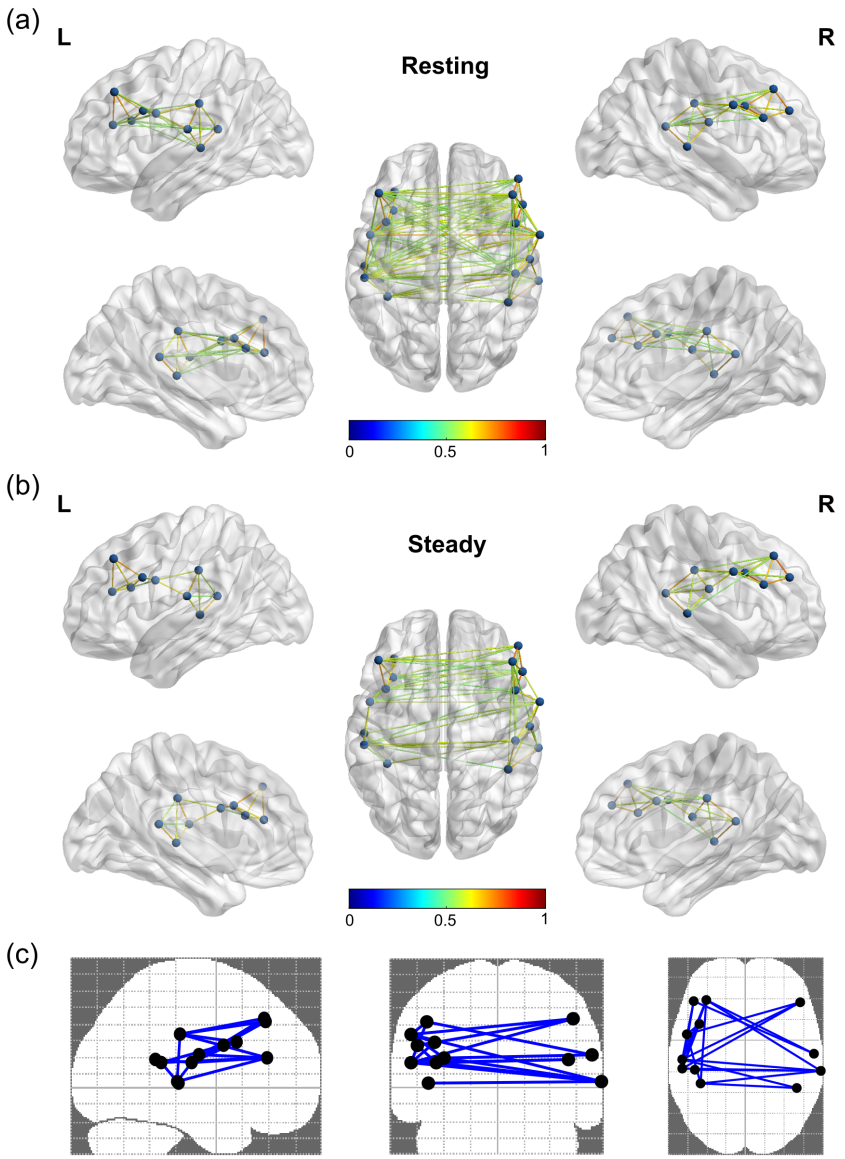

FIGURE 5 Group-level weighted connectivity maps after retaining supra-thresholded weights with a correlation cutoff of 0.5 in (a) resting and (b) steady states. The connections from lateral and medial views are shown on the left and right side of the panel for each hemisphere and the dorsal view is displayed in the centre of each panel. (c) Visualization of functional links with significantly higher connectivity strength in resting state than steady state. The results were obtained from NBS toolbox (Zalesky, Fornito, Harding, et al., 2010).

qualitative results, long-distance inter-hemispheric links in both frontal and temporal brain areas and intra-hemispheric long-range connections between left frontal and left temporal regions demonstrated significantly higher connectivity strengths in resting state than steady state (lowest p value: 0.0058). No significant effect was found for connections within the right hemisphere between frontal and temporal areas as shown in Figure 5c. Out of 12 nodes associated with a significant effect (marked as black filled circles), eight were in the left hemisphere while the remaining four were in the right hemisphere. The NBS results further revealed that 10 edges (out of a total of 21 significant edges) were in the left hemisphere with an overwhelming majority being long-range connections between left frontal and left temporal regions, exhibiting a strong leftward asymmetry in the resting state condition. Overall, we could observe a strong alignment between qualitative and quantitative results in terms of general patterns of connectivity differences between resting and steady states.

3.4 | Differences of functional integration and segregation across resting and steady states emerge after the first 6-months of life

Despite that many task-related studies have provided the evidence of rapid maturation of language networks due to the exposure of novel auditory input in early childhood, age-related differences from a functional connectivity standpoint are not fully understood. We hypothesized that developmental effects of language networks could be identified by assessing functional differences across experimental conditions (resting and steady) in two subgroups of participants aged (1) 6-months or below and (2) above 6-months. To test this hypothesis, we used the same analytical framework described in Section 2.5 with normalized global efficiency and clustering coefficient as a measure of functional integration and segregation, respectively. By using the means of normalized network parameters as threshold-agnostic scalars, we aimed to not only minimize the effect of spurious and

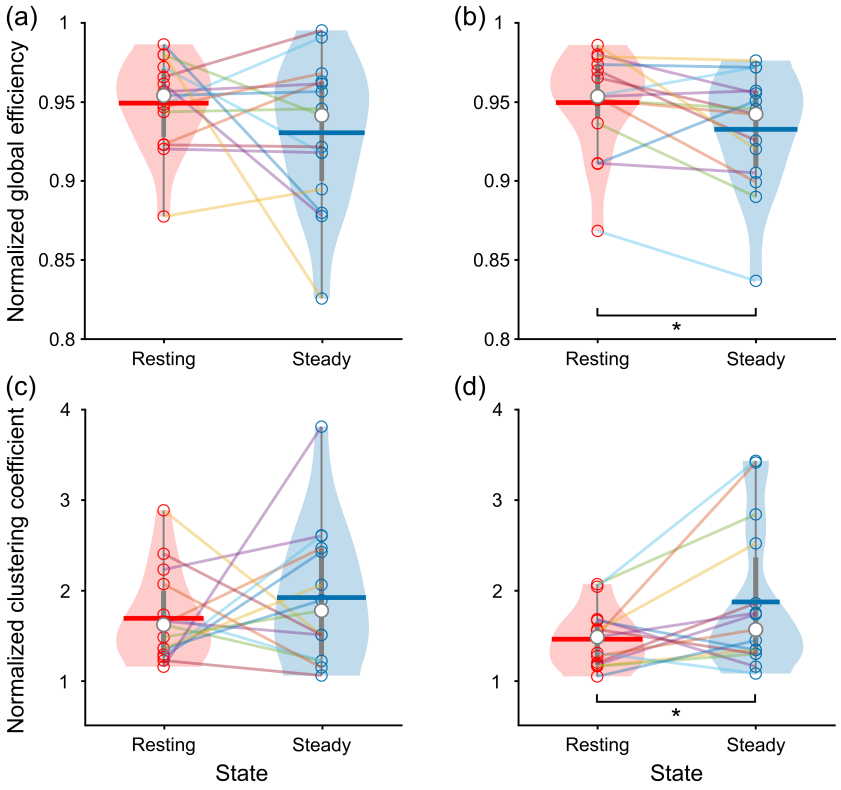

FIGURE 6 Violin plots of normalized mean global efficiency (measure of functional integration) for infants aged (a) 6-months or below and (b) above 6-months in the top panel, and normalized mean clustering coefficient (measure of functional segregation) for infants aged (c) 6-months or below and (d) above 6-months in the bottom panel. Horizontal bold lines indicate group mean and white filled circles denote median of each network metric. Non-parametric statistical tests were conducted using one-sided paired Wilcoxon signed-rank test and the notation * indicates $p < 0.05$.

weak connections but also reduce the dependence of study conclusions on the selection choice of a single threshold.

The general trends observed in normalized global efficiency and clustering coefficient including all participants remained the same for both 6-months or below and above 6-months age groups when investigated separately. Higher normalized global efficiency was observed on average in resting state compared to steady state for both age groups (Figure 6). The normalized metrics represent the factor of change of measures in real network relative to matched random networks. A value much smaller than one in global efficiency indicates that the network topology of real networks deviates further away from random networks but closer towards regular networks, which have high clustering coefficients and long average path lengths, as observed in steady state. While multiple dynamics were observed in the group of infants aged 6-months or below, a large majority of subjects (12 out of 15 or 80%) above 6-months showed a decrease in normalized global efficiency from resting to steady state (Figure S2). From the statistical analysis, no significant effect was found for younger cohort of 6-months or below ($Z = 0.37$, $p = 0.36$) while paired Wilcoxon signed rank test yielded a significantly higher global efficiency in resting state than steady state for infants above 6-months of age ($Z = 2.19$, $p = 0.01$). The participant-averaged normalized clustering coefficient was lower in resting state compared to steady state for both age groups, consistent with our findings reported in Section 3.2. A normalized clustering coefficient much higher than one reflects properties of greater deviation from comparable random networks. We have observed this phenomenon indicating the topology of real networks is more intermediate between regular and random networks in steady state compared to resting state.

Similar to the previous case, a large proportion of infants above 6-months of age exhibited higher normalized clustering coefficient in steady state than resting state (11 out of 15 or 73%) as shown in Figure S3. A Wilcoxon signed rank test was performed to test paired differences in median of normalized clustering coefficients across resting and steady states for two age groups separately. The statistical results revealed a significantly lower normalized clustering coefficient in resting than steady state in the older cohort of infants above 6-months ($Z = -2.02$, $p = 0.02$), but not for infants aged 6-months or below ($Z = -0.60$, $p = 0.28$). These results suggest that there is no detectable topological difference in language networks of younger infants in terms of functional integration and segregation for experimental conditions of resting and steady state. However, topological differences which support information processing across distributed language regions and speech sound processing within local clusters tends to appear in infants above 6-months of age. This could be because language networks maintain a delicate balance between global integration and local segregation during early infancy. However, as infants get exposed to novel auditory input and develop speech and language skills, language networks exhibit more distinct features in functional topology.

4 | DISCUSSION

4.1 | Small-world topology of language networks in infants

Following the discovery of small world topology of brain networks in animal studies, both structural and functional neuroimaging studies

with humans have also shown that similar properties exist in human brains (Bassett & Bullmore, 2017; Bullmore & Sporns, 2009). Recent advances in high precision tract-tracing studies and computational modelling have provided evidence in support of this hypothesis demonstrating functionally important properties of near-random path lengths and non-random clustering (Bassett & Bullmore, 2017; Bullmore & Bassett, 2011; Bullmore & Sporns, 2012). However, most previous studies have focused on studying the economic small-world properties of brain networks using resting state functional neuroimaging data of adults (Niu et al., 2012), young children (Cai et al., 2018) and infants (Gao et al., 2011; Liu et al., 2022; Zhang et al., 2019). There has been no attempt to directly investigate the small-worldness of language networks in infants under different experimental conditions to the best of our knowledge. In this study, we demonstrated that language networks of babies below 2 years of age have economic properties of small world in both resting and steady states. The results support our hypothesis that language networks of infants can process information in a parallel and distributed manner at a low wiring cost. The small-world topology is an attractive network model for language networks as it is economical in terms of maximizing the information processing efficiency while minimizing wiring costs, supporting the idea of concurrent integrated and segregated information processing.

From an evolutionary point of view, it has been argued that the small-world topology is an economically viable architecture for brain networks (Achard & Bullmore, 2007). It is likely that brain networks have been competitively selected in such a way to minimize the cost of wiring while maximizing the efficiency of information processing. These economical properties are achieved by highly clustered short-range connections and a few selected long-range links which facilitate distributed information processing. While a network with small-world topology is more efficient in terms of information processing compared to a random network, it is also more resilient against random errors and targeted attacks than a regular network (Bassett & Bullmore, 2006; Bullmore & Sporns, 2009; Rubinov & Sporns, 2010), usually indicating the robustness of the network to adapt and reorganize in response to a selectively damaging or disruptive event. These observations collectively suggest that brain networks might have adopted small-world properties due to the selection pressure of brain evolution to achieve the best of both regular and random networks and increased flexibility and adaptability for complex and dynamic behaviours.

4.2 | Methodological motivations of graph network measures

The characteristic path length and global efficiency are two metrics commonly used to measure functional integration. It is understood that these two metrics convey very similar information as they are inversely related. However, path length provides insights on serial information transfer capacity of the network while global efficiency measures parallel information transfer through a series of multiple edges (Achard & Bullmore, 2007; Rubinov & Sporns, 2010). This implies that the characteristic path length is primarily driven by longer paths and global efficiency is influenced more by shorter paths. Furthermore, the average shortest path length was first defined for fully connected graphs meaning that all nodes are connected to a large cluster or subgraph. However, it is common to expect some nodes to be disconnected from main clusters when applying high threshold cut-offs to isolate the strongest connections. In this case, the path length between the disconnected region and other nodes becomes infinite (illustrative theoretical extreme) but due to the inverse relationship, the contribution of this to the global efficiency of the network will be zero. Therefore, using global efficiency as a measure of functional integration not only simplifies the numerical calculations in network analysis but also makes the information flow of the network more interpretable, especially for graphs with disconnected regions.

The clustering coefficient is a measure of functional segregation which indicates the extent of clustered connectivity around individual regions. While mean clustering coefficient is a common metric used in many studies, it could be disproportionately affected by nodes with a lower degree due to the normalization process (Rubinov & Sporns, 2010). On the other hand, more advanced measures of functional segregation can find the exact size of a cluster rather than simply detecting the presence (or lack thereof) of a cluster. These methods often rely on optimization algorithms to identify optimal modular structures, hence highly computationally intensive. In this study, we chose global efficiency and clustering coefficient as measures of functional integration and segregation, respectively due to their simplicity, interpretability and fair trade-off between computational speed and accuracy.

It should be noted that while small-world topology is an interesting and heavily adopted concept in network neuroscience, it does not provide us with meaningful information about the physical layout of nodes and edges embedded in anatomical space (Bassett & Bullmore, 2017). Therefore, it is important to integrate the topology of small-worldness with anatomical information. It has been shown that network metrics such as characteristic path length and clustering coefficient have a strong relationship with the anatomy of the brain (Achard & Bullmore, 2007). For instance, edges in a cluster of nodes have shorter distances whereas edges that traverse longer distances tend to span across distributed regions. While physical distances between nodes (lengths of axonal tracts) are usually not very well-known, Euclidean distance between nodes can be used as a proxy for wiring cost. The optode montage used in our study covered only a narrow area related to auditory and language processing. Although the exact brain regions could not be determined, channel registration information shown in Table 1 indicates that nodes are embedded in the expected anatomical space with reasonably high specificity. However, in the future, brain imaging studies with the integration of more accurate spatial information could enhance our understanding of how structural constraints influence the topological organization of functional networks.

4.3 | Effects of thresholding

During network construction stage, thresholding is a common practice to derive an adjacency matrix from the association matrix. The reason for thresholding is usually to minimize the effect of confounding effects such as spurious correlations due to systematic noise and/or weak functional connections (Bullmore & Bassett, 2011; Bullmore & Sporns, 2009). Since the threshold has a direct influence on the sparsity/density of the resultant network, even having the same threshold could lead to different network topologies in different groups and confound between-group comparisons in most studies. Some studies have adopted analysis techniques that do not strictly require thresholding as a preliminary processing step. For example, principal component analysis can be applied to wavelet correlation matrices to generate frequency-specific eigen images (Achard & Bullmore, 2007). The problem of arbitrariness of setting a single threshold can be tackled to a certain extent by computing network metrics over a broad range of plausible thresholds. In this study, we were interested in investigating within-subject topological differences between two experimental conditions, hence we opted to compute network metrics as a function of all positive correlation thresholds. We aimed to assess differences in absolute network organization between resting and steady states while excluding negative correlations for which interpretation is currently controversial and not straightforward (Fox et al., 2009; Weissenbacher et al., 2009). These limitations call for further research on developing objective methods for threshold selection and investigating the effect of negative correlations on network properties.

4.4 | Binary versus weighted graphs

Another key consideration in graph network analysis is whether to use binary or weighted version of graphs. For networks that are embedded in physical space such as brain networks, measures of anatomical distance between nodes are suitable as weighting factors to construct weighted graphs (Achard & Bullmore, 2007). However, as the exact axonal lengths between different brain regions are hard to predetermine, the use of functional distances is an alternative for weighting matrix. Many previous studies have primarily focused on using binary graphs in most cases due to the simplicity in defining null network models, clarity in the definition of network metrics and lower computational complexity (Bassett & Bullmore, 2017). It is important to note that binary graphs may fail to pick up subtle differences in network organization. The weighted approach could be particularly more useful and powerful when the networks are denser and sensitive to subtle differences. In our study, a supplementary analysis using weighted graphs revealed that the main findings are consistent with those generated from binary graphs. Functional language networks from weighted graphs exhibited economic small-world properties in both resting and steady states as shown in Figure S4 in the supplementary materials. We observed numerically higher functional integration in resting state compared to steady state and numerically lower functional segregation in resting state than steady state. However, the results of this analysis did not reach statistical significance (Figure S5). In this study, we adopted simpler binary approach as the primary analysis as we mainly focused on language areas of the brain. Due to this narrow region of interest, our analysis produced sparser networks which are less sensitive to subtle changes compared to brain-wide large-scale networks.

4.5 | Limitations

Although the chosen sample is a reasonable representation of the cross-sectional population we intended to study, graph network measures of some participants showed considerable variability likely due to individual differences in brain language development and residual physiological and/or measurement noise. We recognize that a longitudinal dataset with bigger sample size would account for such individual variability, improve the statistical power of the study, and provide stronger insights into the evolution of language network topology during early sensitive period of language development.

Following parents' reports indicating no concerns of development, a small proportion of pre-term infants (3 out of 30) were included in the analysis with the corrected gestational age. However, previous studies have found delayed development in primary somatosensory system in pre-term infants even after correcting for age (de Oliveira et al., 2019; Machado et al., 2023). As underlying reasons are not entirely clear, similar deviations may be extended to even higher order networks such as language. Therefore, exclusion of pre-term infants is advisable in future studies when such unaccounted effects cannot be adequately explained.

We note that averaging network metrics over the full range of positive correlations may have reduced the sensitivity of detecting differences between conditions and resulted in limited interpretation. At low thresholds, networks become artificially denser due to small signal fluctuations, thus their degree distribution resembles a random network. As thresholds increase, networks become sparser and more heterogeneous, shifting the network towards a more complex architecture demonstrating small world properties. While results with our approach indicate expected differences between the two conditions, it is worth exploring different ways of selecting an appropriate threshold range to extract distinctions between conditions more effectively.

5 | CONCLUSION

In this study, we compared topological differences of language networks between resting condition and in response to continuous repetitive speech sounds in children aged below 2 years using functional connectivity-based graph network measures. By comparing group-level graph network measures of real networks with respect to matched random networks, we found that functional networks of language demonstrate properties of economic small-world organization in both resting and steady states. From within-subject pairwise

comparisons across two experimental conditions, the results indicated that infants have more functionally integrated networks in resting state compared to steady state to potentially facilitate efficient information transfer across distributed language regions. Language networks in steady state are more functionally segregated, likely allowing information processing to occur within densely interconnected regions highly specialized for speech processing. Finally, the findings from secondary analysis that investigated developmental effects suggested that topological differences in functional integration and segregation can be reliably detected after the first 6-months of life.

ACKNOWLEDGMENTS

Ishara Paranawithana was supported by an Australian Government Research Training Program (RTP) Scholarship and Monash University Postgraduate Publications Award (PPA). The project was funded by grants from the National Health and Medical Research Council of Australia (GNT1154233), the Medical Research Future Fund (BioMedTech Horizons Program) through the Australian Government and the Victorian Medical Research Acceleration Fund. The Bionics Institute acknowledges the support it receives from the Victorian Government through its Operational Infrastructure Support Program. The authors would like to thank the clinical team of Human Hearing Research Group at the Bionics Institute for their help in participant recruitment and data collection. Open access publishing facilitated by Monash University, as part of the Wiley - Monash University agreement via the Council of Australian University Librarians.

CONFLICT OF INTEREST STATEMENT

The authors declare no conflict of interest.

DATA AVAILABILITY STATEMENT

Anonymized data supporting the findings of this study can be made available to interested parties, subject to conditions of research ethics and restrictions according to participant consent.

ORCID

Ishara Paranawithana https://orcid.org/0000-0001-6509-9687

REFERENCES

Aarabi, A., & Huppert, T. J. (2019). Assessment of the effect of data length on the reliability of resting-state fNIRS connectivity measures and graph metrics. *Biomedical Signal Processing and Control*, *54*, 101612.

Achard, S., & Bullmore, E. (2007). Efficiency and cost of economical brain functional networks. *PLoS Computational Biology*, *3*(2), e17.

Aslin, R. N. (1980). Some developmental processes in speech perception. *Child Phonology*, *2*, 67–96.

Ayaz, H., Baker, W. B., Blaney, G., Boas, D. A., Bortfeld, H., Brady, K., Brake, J., Brigadoi, S., Buckley, E. M., & Carp, S. A. (2022). Optical imaging and spectroscopy for the study of the human brain: Status report. *Neurophotonics*, *9*(S2), S24001.

Bassett, D. S., & Bullmore, E. (2006). Small-world brain networks. *The Neuroscientist*, *12*(6), 512–523.

Bassett, D. S., & Bullmore, E. T. (2009). Human brain networks in health and disease. *Current Opinion in Neurology*, *22*(4), 340–347.

Bassett, D. S., & Bullmore, E. T. (2017). Small-world brain networks revisited. *The Neuroscientist*, *23*(5), 499–516.

Biswal, B., Zerrin Yetkin, F., Haughton, V. M., & Hyde, J. S. (1995). Functional connectivity in the motor cortex of resting human brain using echo-planar MRI. *Magnetic Resonance in Medicine*, *34*(4), 537–541.

Blanco, B., Molnar, M., Carreiras, M., Collins-Jones, L. H., Rosas, E. E. V., Cooper, R. J., & Caballero-Gaudes, C. (2021). Group-level cortical functional connectivity patterns using fNIRS: Assessing the effect of bilingualism in young infants. *Neurophotonics*, *8*(2), 025011.

Bulgarelli, C., Blasi, A., Arridge, S., Powell, S., de Klerk, C. C., Southgate, V., Brigadoi, S., Penny, W., Tak, S., & Hamilton, A. (2018). Dynamic causal modelling on infant fNIRS data: A validation study on a simultaneously recorded fNIRS-fMRI dataset. *NeuroImage*, *175*, 413–424.

Bulgarelli, C., de Klerk, C. C., Richards, J. E., Southgate, V., Hamilton, A., & Blasi, A. (2020). The developmental trajectory of fronto-temporoparietal connectivity as a proxy of the default mode network: A longitudinal fNIRS investigation. *Human Brain Mapping*, *41*, 2717–2740.

Bullmore, E., & Sporns, O. (2009). Complex brain networks: Graph theoretical analysis of structural and functional systems. *Nature Reviews Neuroscience*, *10*(3), 186–198.

Bullmore, E., & Sporns, O. (2012). The economy of brain network organization. *Nature Reviews Neuroscience*, *13*(5), 336–349.

Bullmore, E. T., & Bassett, D. S. (2011). Brain graphs: Graphical models of the human brain connectome. *Annual Review of Clinical Psychology*, *7*, 113–140.

Bullmore, E. T., Suckling, J., Overmeyer, S., Rabe-Hesketh, S., Taylor, E., & Brammer, M. J. (1999). Global, voxel, and cluster tests, by theory and permutation, for a difference between two groups of structural MR images of the brain. *IEEE Transactions on Medical Imaging*, *18*(1), 32–42.

Cai, L., Dong, Q., & Niu, H. (2018). The development of functional network organization in early childhood and early adolescence: A resting-state fNIRS study. *Developmental Cognitive Neuroscience*, *30*, 223–235.

de la Cruz-Pavía, I., & Gervain, J. (2023). Six-month-old infants' perception of structural regularities in speech. *Cognition*, *238*, 105526.

de Oliveira, S. R., Machado, A. C. C., de Paula, J. J., Novi, S. L., Mesquita, R. C., de Miranda, D. M., & Bouzada, M. C. F. (2019). Changes of functional response in sensorimotor cortex of preterm and full-term infants during the first year: An fNIRS study. *Early Human Development*, *133*, 23–28.

Dehaene-Lambertz, G., Hertz-Pannier, L., Dubois, J., Mériaux, S., Roche, A., Sigman, M., & Dehaene, S. (2006). Functional organization of perisylvian activation during presentation of sentences in preverbal infants. *Proceedings of the National Academy of Sciences*, *103*(38), 14240–14245.

Delpy, D. T., Cope, M., van der Zee, P., Arridge, S., Wray, S., & Wyatt, J. (1988). Estimation of optical pathlength through tissue from direct time of flight measurement. *Physics in Medicine & Biology*, *33*(12), 1433–1442.

Dennis, E. L., & Thompson, P. M. (2014). Functional brain connectivity using fMRI in aging and Alzheimer's disease. *Neuropsychology Review*, *24*(1), 49–62.

Duan, L., Zhang, Y.-J., & Zhu, C.-Z. (2012). Quantitative comparison of resting-state functional connectivity derived from fNIRS and fMRI: A simultaneous recording study. *NeuroImage*, *60*(4), 2008–2018.

Emerson, R. W., Gao, W., & Lin, W. (2016). Longitudinal study of the emerging functional connectivity asymmetry of primary language regions during infancy. *Journal of Neuroscience*, *36*(42), 10883–10892.

Ferrari, M., & Quaresima, V. (2012). A brief review on the history of human functional near-infrared spectroscopy (fNIRS) development and fields of application. *NeuroImage*, *63*(2), 921–935.

Fishburn, F. A., Ludlum, R. S., Vaidya, C. J., & Medvedev, A. V. (2019). Temporal derivative distribution repair (TDDR): A motion correction method for fNIRS. *NeuroImage*, *184*, 171–179.

Fox, M. D., & Greicius, M. (2010). Clinical applications of resting state functional connectivity. *Frontiers in Systems Neuroscience*, *4*, 1443.

Fox, M. D., & Raichle, M. E. (2007). Spontaneous fluctuations in brain activity observed with functional magnetic resonance imaging. *Nature Reviews Neuroscience*, *8*(9), 700–711.

Fox, M. D., Zhang, D., Snyder, A. Z., & Raichle, M. E. (2009). The global signal and observed anticorrelated resting state brain networks. *Journal of Neurophysiology*, *101*(6), 3270–3283.

Friederici, A. D. (2012). The cortical language circuit: From auditory perception to sentence comprehension. *Trends in Cognitive Sciences*, *16*(5), 262–268.

Fu, X., & Richards, J. E. (2021). devfOLD: A toolbox for designing age-specific fNIRS channel placement. *Neurophotonics*, *8*(4), 045003.

Gao, W., Alcauter, S., Smith, J. K., Gilmore, J. H., & Lin, W. (2015). Development of human brain cortical network architecture during infancy. *Brain Structure and Function*, *220*(2), 1173–1186.

Gao, W., Gilmore, J. H., Giovanello, K. S., Smith, J. K., Shen, D., Zhu, H., & Lin, W. (2011). Temporal and spatial evolution of brain network topology during the first two years of life. *PLoS One*, *6*(9), e25278.

Hickok, G., & Poeppel, D. (2007). The cortical organization of speech processing. *Nature Reviews*, *8*(5), 393–402.

Homae, F., Watanabe, H., Otobe, T., Nakano, T., Go, T., Konishi, Y., & Taga, G. (2010). Development of global cortical networks in early infancy. *Journal of Neuroscience*, *30*(14), 4877–4882.

Hu, Z., Liu, G., Dong, Q., & Niu, H. (2020). Applications of resting-state fNIRS in the developing brain: A review from the connectome perspective. *Frontiers in Neuroscience*, *14*, 476.

Jung, M. E., Colletta, M., Coalson, R., Schlaggar, B. L., & Lieu, J. E. (2017). Differences in interregional brain connectivity in children with unilateral hearing loss. *The Laryngoscope*, *127*(11), 2636–2645.

Liu, G., Huo, E., Liu, H., Jia, G., Zhi, Y., Dong, Q., & Niu, H. (2022). Development and emergence of functional network asymmetry in 3-to 9-month-old infants. *Cortex*, *154*, 390–404.

Lu, C.-M., Zhang, Y.-J., Biswal, B. B., Zang, Y.-F., Peng, D.-L., & Zhu, C.-Z. (2010). Use of fNIRS to assess resting state functional connectivity. *Journal of Neuroscience Methods*, *186*(2), 242–249.

Machado, A. C. C. d. P., Magalhães, L. d. C., de Oliveira, S. R., Novi, S. L., Mesquita, R. C., de Miranda, D. M., & Bouzada, M. C. F. (2023). Can tactile reactivity in preterm born infants be explained by an immature cortical response to tactile stimulation in the first year? A pilot study. *Journal of Perinatology*, *43*(6), 728–734.

Mao, D., Wunderlich, J., Savkovic, B., Jeffreys, E., Nicholls, N., Lee, O. W., Eager, M., & McKay, C. M. (2021). Speech token detection and discrimination in individual infants using functional near-infrared spectroscopy. *Scientific Reports*, *11*(1), 1–14.

McKay, C., Wunderlich, J., Mao, D., Balasubramanian, G., Lee, O. W., Gao, D., & McDonald, L. (2023). A reliable, accurate, and clinic-friendly objective test of speech sound detection and discrimination in sleeping infants.

Nakano, T., Watanabe, H., Homae, F., & Taga, G. (2009). Prefrontal cortical involvement in young infants' analysis of novelty. *Cerebral Cortex*, *19*(2), 455–463.

NeuroImaging Tools and Resources Collaboratory. (2023). Functional Connectivity Analysis Tool for near-infrared spectroscopy data. https://www.nitrc.org/projects/fcnirs

Niu, H., Li, Z., Liao, X., Wang, J., Zhao, T., Shu, N., Zhao, X., & He, Y. (2013). Test-retest reliability of graph metrics in functional brain networks: A resting-state fNIRS study. *PLoS One*, *8*(9), e72425.

Niu, H., Wang, J., Zhao, T., Shu, N., & He, Y. (2012). Revealing topological organization of human brain functional networks with resting-state functional near infrared spectroscopy. *PLoS One*, *7*(9), e45771.

Oldham, S., & Fornito, A. (2019). The development of brain network hubs. *Developmental Cognitive Neuroscience*, *36*, 100607.

Paranawithana, I., Mao, D., McKay, C. M., & Wong, Y. T. (2023a). Connections between spatially distant primary language regions strengthen with age during infancy, as revealed by resting state fNIRS. *Journal of Neural Engineering*, *20*, 016053.

Paranawithana, I., Mao, D., McKay, C. M., & Wong, Y. T. (2023b). Investigating the effect of data length on the performance of frequency-domain fNIRS functional connectivity measures. 2023 45th annual international conference of the IEEE engineering in Medicine & Biology Society (EMBC), IEEE.

Paranawithana, I., Mao, D., Wong, Y. T., & McKay, C. M. (2022). Reducing false discoveries in resting-state functional connectivity using short channel correction: An fNIRS study. *Neurophotonics*, *9*(1), 015001.

Pinti, P., Tachtsidis, I., Hamilton, A., Hirsch, J., Aichelburg, C., Gilbert, S., & Burgess, P. W. (2020). The present and future use of functional near-infrared spectroscopy (fNIRS) for cognitive neuroscience. *Annals of the New York Academy of Sciences*, *1464*(1), 5–29.

Polka, L., & Werker, J. F. (1994). Developmental changes in perception of nonnative vowel contrasts. *Journal of Experimental Psychology: Human Perception and Performance*, *20*(2), 421.

Rubinov, M., & Sporns, O. (2010). Complex network measures of brain connectivity: Uses and interpretations. *NeuroImage*, *52*(3), 1059–1069.

Saffran, J. R., Aslin, R. N., & Newport, E. L. (1996). Statistical learning by 8-month-old infants. *Science*, *274*(5294), 1926–1928.

Santosa, H., Zhai, X., Fishburn, F., & Huppert, T. (2018). The NIRS brain AnalyzIR toolbox. *Algorithms*, *11*(5), 73.

Scholkmann, F., Kleiser, S., Metz, A. J., Zimmermann, R., Pavia, J. M., Wolf, U., & Wolf, M. (2014). A review on continuous wave functional near-infrared spectroscopy and imaging instrumentation and methodology. *NeuroImage*, *85*, 6–27.

Shader, M. J., Luke, R., Gouailhardou, N., & McKay, C. M. (2021). The use of broad vs restricted regions of interest in functional near-infrared spectroscopy for measuring cortical activation to auditory-only and visual-only speech. *Hearing Research*, *406*, 108256.

Sharma, A., & Cardon, G. (2014). *Developmental plasticity of the central auditory system: Evidence from deaf children fitted with cochlear implants* (pp. 315–337). Development of Auditory and Vestibular Systems, Elsevier.

Shi, B., Yang, L.-Z., Liu, Y., Zhao, S.-L., Wang, Y., Gu, F., Yang, Z., Zhou, Y., Zhang, P., & Zhang, X. (2016). Early-onset hearing loss reorganizes the visual and auditory network in children without cochlear implantation. *Neuroreport*, *27*(3), 197–202.

Wang, S., Chen, B., Yu, Y., Yang, H., Cui, W., Li, J., & Fan, G. G. (2019). Alterations of structural and functional connectivity in profound sensorineural hearing loss infants within an early sensitive period: A combined DTI and fMRI study. *Developmental Cognitive Neuroscience*, *38*, 100654.

Weiss-Croft, L. J., & Baldeweg, T. (2015). Maturation of language networks in children: A systematic review of 22 years of functional MRI. *NeuroImage*, *123*, 269–281.

Weissenbacher, A., Kasess, C., Gerstl, F., Lanzenberger, R., Moser, E., & Windischberger, C. (2009). Correlations and anticorrelations in resting-state functional connectivity MRI: A quantitative comparison of preprocessing strategies. *NeuroImage*, *47*(4), 1408–1416.

Werker, J. F. (2024). Phonetic perceptual reorganization across the first year of life: Looking back. *Infant Behavior and Development*, *75*, 101935.

Werker, J. F., & Tees, R. C. (1984). Cross-language speech perception: Evidence for perceptual reorganization during the first year of life. *Infant Behavior and Development*, *7*(1), 49–63.

White, B. R., Snyder, A. Z., Cohen, A. L., Petersen, S. E., Raichle, M. E., Schlaggar, B. L., & Culver, J. P. (2009). Resting-state functional connectivity in the human brain revealed with diffuse optical tomography. *NeuroImage*, *47*(1), 148–156.

Xia, M., Wang, J., & He, Y. (2013). BrainNet viewer: A network visualization tool for human brain connectomics. *PLoS One*, *8*(7), e68910.

Xu, J., Liu, X., Zhang, J., Li, Z., Wang, X., Fang, F., & Niu, H. (2015). FC-NIRS: A functional connectivity analysis tool for near-infrared spectroscopy data. *BioMed Research International*, *2015*(1), 248724.

Zalesky, A., Fornito, A., & Bullmore, E. T. (2010). Network-based statistic: Identifying differences in brain networks. *NeuroImage*, *53*(4), 1197–1207.

Zalesky, A., Fornito, A., Harding, I. H., Cocchi, L., Yücel, M., Pantelis, C., & Bullmore, E. T. (2010). Whole-brain anatomical networks: Does the choice of nodes matter? *NeuroImage*, *50*(3), 970–983.

Zhang, F., Moerman, F., Niu, H., Warreyn, P., & Roeyers, H. (2022). Atypical brain network development of infants at elevated likelihood for autism spectrum disorder during the first year of life. *Autism Research*, *15*, 2223–2237.

Zhang, H., Shen, D., & Lin, W. (2019). Resting-state functional MRI studies on infant brains: A decade of gap-filling efforts. *NeuroImage*, *185*, 664–684.

Zhang, H., Zhang, Y.-J., Lu, C.-M., Ma, S.-Y., Zang, Y.-F., & Zhu, C.-Z. (2010). Functional connectivity as revealed by independent component analysis of resting-state fNIRS measurements. *NeuroImage*, *51*(3), 1150–1161.

Zhang, Y., Mao, Z., Feng, S., Liu, X., Lan, L., Zhang, J., & Yu, X. (2018). Altered functional networks in long-term unilateral hearing loss: A connectome analysis. *Brain and Behavior*, *8*(2), e00912.

Zhang, Y.-J., Lu, C.-M., Biswal, B. B., Zang, Y.-F., Peng, D., & Zhu, C.-Z. (2010). Detecting resting-state functional connectivity in the language system using functional near-infrared spectroscopy. *Journal of Biomedical Optics*, *15*(4), 047003.

SUPPORTING INFORMATION

Additional supporting information can be found online in the Supporting Information section at the end of this article.

How to cite this article: Paranawithana, I., Mao, D., McKay, C. M., & Wong, Y. T. (2024). Language networks of normal-hearing infants exhibit topological differences between resting and steady states: An fNIRS functional connectivity study. *Human Brain Mapping*, *45*(13), e70021. https://doi.org/10.1002/hbm.70021